Published by :
https://www.ijert.org/
An International Peer-Reviewed Journal

International Journal of Engineering Research & Technology (IJERT)
ISSN: 2278-0181
Vol. 15 Issue 06 , June - 2026

Comparative Photocatalytic Degradation of Domestic Grey Wastewater Using Undoped and 4% Nickel-Doped TiO_2 Nanoparticles Synthesized via Microwave-Assisted Sol - Gel Route

Himani Pachauri[1], Ashish Kumar[2], Shivalini Singh, Mohammad Mudassir
Department of Chemistry, Agra College, Agra
(Dr. Bhim Rao Ambedkar University, Agra – 282001)

Abstract **- Greywater reuse is increasingly recognised as a critical component of sustainable domestic water management, but conventional treatment is often insufficient to remove the surfactant-derived organic and chromophoric load characteristic of laundry and bathing effluent. In this study, undoped TiO_2 and 4 wt.% nickel-doped TiO_2 (4% Ni–TiO_2) nanoparticles were synthesised by a microwave-assisted sol–gel route using starch as a green capping agent, and evaluated as heterogeneous photocatalysts for the degradation of synthetic domestic grey wastewater (pH 8.2, turbidity 45 NTU, chemical oxygen demand (COD) 530 mg/L, total organic carbon (TOC) 178 mg/L, UV_{254} 0.973 cm^{-1}) under UV irradiation (365 nm) in a flat-bed open-dish laminar-air-flow reactor. Photocatalytic trials were conducted at three catalyst doses (10, 30 and 50 mg/100 mL) and four irradiation times (60–180 min), with COD, TOC, UV_{254} absorbance and turbidity monitored in triplicate (n = 3). Control experiments confirmed matrix stability (<2% drift), quantified the contribution of direct photolysis (largest for UV_{254}, 40.0%) and dark adsorption (~25% for both catalysts), allowing the genuine photocatalytic contribution to be deconvoluted from the total observed removal. At the optimal dose of 30 mg/100 mL and 180 min, 4% Ni–TiO_2 substantially outperformed undoped TiO_2 across all four parameters, achieving 83.3 ± 0.9% COD removal, 85.8 ± 0.8% TOC removal, 85.8 ± 0.4% UV_{254} removal and 87.7 ± 1.5% turbidity removal, compared with only 42.0 ± 0.5%, 39.8 ± 0.7%, 45.0 ± 1.1% and 49.1 ± 1.3%, respectively, for undoped TiO_2. Pseudo-first-order kinetic modelling ($R^2 \geq 0.999$ for both catalysts) gave a COD rate constant for 4% Ni–TiO_2 (9.93×10^{-3} min^{-1}) more than three times that of undoped TiO_2 (3.04×10^{-3} min^{-1}). One-way ANOVA and Tukey HSD post-hoc analysis confirmed these differences were statistically significant ($p < 0.01$). The superior performance of 4% Ni–TiO_2 is attributed to a brookite–anatase heterojunction that suppresses electron–hole recombination, a markedly smaller crystallite size (7.54 nm vs. 15.0 nm for undoped TiO_2, corroborated by single-peak Scherrer analysis of the raw XRD data), and a substantially narrowed optical band gap (2.57 eV vs. 3.06 eV by Tauc analysis of UV–Vis diffuse reflectance spectra), which together increase hydroxyl-radical generation, visible-light harvesting and specific surface area available for pollutant adsorption and oxidation. These findings identify 4% Ni–TiO_2 as a high-performing, low-cost candidate for the photocatalytic treatment of real-world domestic grey wastewater.**

Keywords **- TiO_2 photocatalysis; nickel doping; grey wastewater treatment; sol–gel synthesis; pseudo-first-order kinetics; advanced oxidation process**

1. INTRODUCTION

The increasing discharge of organic pollutants in aquatic environments is an urgent environmental concern, and the conventional wastewater treatment methods - biological oxidation, coagulation-flocculation and activated-carbon adsorption - are often inefficient for the complete mineralisation of recalcitrant organic compounds, which stimulates the development of advanced oxidation processes (AOPs) capable of non-selective degradation. Heterogeneous photocatalysis involving titanium dioxide (TiO_2) has attracted much attention as an effective AOP due to its chemical stability, non-toxicity, low cost and strong oxidising power under UV irradiation. However, the wide bandgap of anatase TiO_2 (≈ 3.0–3.2 eV) restricts photoactivity mainly to the UV region, which accounts for only about 5% of the solar spectrum. A well-established approach to overcome this constraint is transition-metal doping which introduces impurity energy levels within the bandgap to increase the light absorption and decrease electron–hole recombination.

Domestic grey wastewater, which is the combined effluent from laundry, bathing and handwashing, is one of the largest and most easily recoverable fractions of household water demand, but the load of surfactant, detergent-builder and personal-care-product makes it ill-suited to direct reuse or discharge without treatment. The conventional biological treatment is sometimes hindered by the toxicity of surfactants at the concentrations commonly present in these streams, resulting in increased interest in advanced oxidation processes (AOPs) that are not dependent on microbial activity [13]. Among AOPs, heterogeneous photocatalysis based on TiO_2 is particularly

International Journal of Engineering Research & Technology (IJERT)
ISSN: 2278-0181
Vol. 15 Issue 06 , June - 2026

attractive because of its chemical stability, non-toxicity, low cost, and ability to non-selectively mineralise both aromatic and aliphatic organic contaminants via photogenerated hydroxyl radicals (•OH) and superoxide radical anions ($O_2^{\bullet-}$). However, a persistent constraint of undoped (unmodified) TiO_2 is the high recombination rate of photogenerated electron–hole pairs under UV irradiation, which results in a significant decrease in the quantum efficiency for radical generation. A well-known approach to circumvent this problem is doping with transition-metals: dopant ions can induce intra-gap trap states or heterojunction band alignments to spatially separate photogenerated charge carriers, thereby prolonging their lifetime and boosting the yield of surface-bound reactive oxygen species. In particular, nickel doping has been correlated with the creation of a brookite–anatase heterojunction, and favourable Ni 2+ /Ni 3+ trap-state energetics, both of which are expected to improve charge separation compared to the pure anatase phase.

This study presents a direct, quantitative comparison between undoped TiO_2 and 4 wt.% Ni–TiO_2 for grey wastewater remediation. Undoped TiO_2 serves as the essential baseline against which the magnitude of dopant-derived enhancement can be benchmarked, while 4% Ni–TiO_2 was identified as good performer for TOC mineralisation. The objective of this work is therefore to (i) characterise the structural differences between the two catalysts, (ii) quantify their comparative photocatalytic performance across four complementary water-quality parameters under identical reactor conditions, (iii) deconvolute genuine photocatalytic activity from non-catalytic removal pathways, and (iv) rationalise the observed performance gap in terms of the underlying charge-separation mechanism. In this work, both undoped and Ni doped TiO2 are analysed, including structure, techniques of manufacturing and photocatalytic activity. There are three main polymorphs: the anatase, rutile and brookite. Anatase possesses the highest photocatalytic activity owing to its higher bandgap (~3.2 eV) and lower charge-carrier recombination rate. The most common synthesis procedure is the sol-gel method. It is characterised by simplicity and control of the composition. Optimum circumstances such as calcination temperature of 673K are very critical for the enhancement of the photocatalytic activity especially for the dye degradation.

The photocatalytic ability of TiO_2 can be improved by doping with transition metals to form impurity states, which extend the absorption to the visible light region and prolong the charge-carrier life-times. However, too much doping can be very detrimental to the performance as it introduces recombination centers. It was shown that doping with different elements like copper, nickel improved the degrading efficiency and nickel doped TiO2 exhibited the highest efficiency because of the minimum crystallite size and superior charge separation. The article also mentions the novel synthesis strategies like microwave assisted and biopolymer assisted synthesis employing starch for reduction of agglomeration and enhancement of photocatalytic performance. Moreover, it indicates the significance of operational parameters such as catalyst dosage and light intensity for the treatment of residential wastewater in real applications.

2. LITERATURE REVIEW

Finally, the noted research need is the lack of comparison studies of different dopants synthesised under similar conditions and tested in complex matrices such as grey water. To address these gaps, the present work was set up to test undoped and 4% nickel doped TiO_2 against a defined wastewater matrix using COD, TOC, UV254 and turbidity as markers for photocatalytic efficacy using a standardised starch templated microwave assisted sol-gel method. The foundations of semiconductor photocatalysis trace back to the discovery of UV-induced water splitting at an illuminated TiO_2 electrode [1], a finding that established TiO_2 as the benchmark photocatalytic material and was later consolidated, together with its mechanistic basis in electron–hole pair generation and hydroxyl-radical-mediated oxidation, in a comprehensive review of semiconductor photocatalysis for environmental remediation [2]. Sol–gel synthesis from titanium alkoxide precursors has since become the most widely used route to nanocrystalline anatase TiO_2 for pollutant degradation, with calcination temperature and synthesis conditions reported to govern crystallite size, surface area and the resulting photocatalytic activity towards chlorophenolic pollutants under solar irradiation [3].

Transition-metal doping of TiO_2 has been extensively investigated as a means of narrowing the band gap and suppressing electron–hole recombination. A direct comparison of pure and metal-ion-doped nanocrystalline titania demonstrated that dopant incorporation systematically red-shifts the optical absorption edge and alters photocatalytic activity relative to the undoped baseline [4], while amorphous TiO_2 doped with trivalent Cr and Fe ions was shown to remain photocatalytically active under both UV and visible light and to be recyclable over repeated cycles [5]. Similarly, cobalt doping of sol–gel-derived TiO_2 nanoparticles was found to reduce crystallite size and modify the optical band gap relative to the undoped material [6], and copper- and zinc-doped TiO_2 nanopowders prepared by a microwave-assisted sol–gel route were reported to retain a single-phase anatase structure with the dopant incorporated at the nanoparticle surface [11]. These studies collectively support the general principle, central to the present work, that transition-metal doping of TiO_2 modifies crystallite size and band gap in a dopant-dependent manner that governs photocatalytic performance.

International Journal of Engineering Research & Technology (IJERT)
ISSN: 2278-0181
Vol. 15 Issue 06 , June - 2026

Microwave-assisted synthesis, the route adopted in the present study, has been reported by several groups to offer faster, more energy-efficient and more uniform heating than conventional oven-drying, with consequent benefits for crystallite-size control. Silver-modified TiO_2 prepared by a sol–gel process using hydrazine as a reducing agent showed enhanced visible-light photocatalytic activity attributable to the silver dopant [7], and a closely related study using a controlled, energy-efficient microwave-assisted route to prepare Ag-doped anatase TiO_2 reported improved photocatalytic performance over a range of silver loadings [8]. The microwave-assisted sol–gel approach has also been extended to zirconium-doped TiO_2 for dye degradation, with the doped nanostructures showing a reduced band gap and increased surface area relative to undoped TiO_2 [9], and to nitrogen doping via a microwave-assisted method for pesticide degradation, which likewise reported enhanced photocatalytic activity relative to the undoped baseline [10]. These microwave-assisted studies provide direct precedent for the synthesis route used in the present work, although none combine microwave processing with a starch-templating step or with nickel as the dopant species, a combination addressed specifically in the present study.

Finally, accurate determination of crystallite size from X-ray diffraction line broadening, central to the structural comparison made in Section 4.1 below, follows the phase-characterisation methodology established for anatase and rutile TiO_2 powders by XRD and transmission electron microscopy [12], which remains a standard reference for Scherrer-based crystallite-size analysis of TiO_2 nanopowders. Taken together, the literature indicates that (i) TiO_2 is a well-established UV-active photocatalyst whose activity can be extended and enhanced through transition-metal doping, (ii) microwave-assisted sol–gel synthesis is an effective, energy-efficient route to nanocrystalline doped TiO_2, and (iii) direct, quantitative comparisons between undoped and nickel-doped TiO_2 synthesised by an identical, starch-templated microwave-assisted protocol and evaluated against a real-world wastewater matrix remain comparatively scarce — the specific gap addressed by the present study.

3. MATERIALS AND METHODS

3.1 Materials

Titanium tetra-isopropoxide (TTIP, $Ti[OCH(CH_3)_2]_4$) was used as the titanium precursor, and nickel(II) nitrate hexahydrate ($Ni(NO_3)_2{\cdot}6H_2O$) as the nickel dopant precursor. Isopropanol, absolute ethanol, deionised water and concentrated nitric acid were used as received for hydrolysis and peptisation. Soluble starch ($(C_6H_{10}O_5)_n$) was used as a green, biodegradable capping/stabilising agent. All synthesis work was carried out in the Department of Chemistry, Agra College, Dr. Bhim Rao Ambedkar University, Agra.

3.2 Catalyst Synthesis

Both undoped TiO_2 and 4% Ni–TiO_2 nanoparticles were prepared by a microwave-assisted, starch-templated sol–gel route [11].

The Ni-doped catalyst was prepared using the modified sol–gel technique. 90 mL of isopropanol was poured to 10 mL of TTIP and agitated for 45 minutes at the beginning. A nickel nitrate solution for 4 wt.% Ni loading was added to commence gelation which resulted in an off-white gel. A 5% starch solution was added to prevent agglomeration and then microwave dried for 20 min. The gel was then milled and calcined at 550°C for 3 h to give a nanocrystalline 4% Ni–TiO2 powder. The same process was followed for the undoped catalyst and for Ni at 4% loading.

Microwave-assisted drying was selected in preference to conventional oven-drying for its rapid, volumetrically uniform heating, which shortens processing time and limits the uncontrolled particle agglomeration and coarsening associated with prolonged conventional thermal treatment, while the starch capping agent was incorporated as a green, low-cost structure-directing template to further moderate nucleation and crystallite growth during calcination [14].

3.3 Catalyst Characterisation

Both catalysts were characterised using X-ray diffraction (XRD; Rigaku MiniFlex 300/600, Cu Kα radiation, $\lambda = 1.5406$ Å, 40 kV/15 mA, $2\theta = 2–90°$, step 0.02°) with Williamson–Hall microstrain analysis to determine crystallite size and lattice strain; UV–Vis diffuse reflectance spectroscopy (DRS; 200–800 nm) with Kubelka–Munk/Tauc plot analysis to determine optical band gap; and field-emission scanning electron microscopy with energy-dispersive X-ray analysis (FESEM/EDAX; Carl Zeiss Sigma 300 FESEM with Oxford Instruments EDAX, Annamalai University) for morphology and elemental composition.

3.4 Grey Wastewater Matrix

Synthetic domestic grey wastewater was used as the model pollutant matrix, formulated to represent combined laundry, bathing and handwashing effluent. The baseline (untreated) physicochemical profile is summarised in Table 1 and served as the common C_0 reference for all percentage-removal and kinetic calculations.

International Journal of Engineering Research & Technology (IJERT)
ISSN: 2278-0181
Vol. 15 Issue 06 , June - 2026

Table 1. Baseline physicochemical characteristics of the untreated synthetic grey wastewater.

Parameter	Value
pH	8.2
Turbidity (NTU)	45
COD (mg/L)	530
TOC (mg/L)	178
UV_{254} (cm^{-1})	0.973

The mildly alkaline baseline pH (8.2) is typical of residual soap, detergent and surfactant content, and places the TiO_2 surface (point of zero charge ≈ 6.0–6.5 for anatase) in a net negative charge state that favours adsorption of cationic and neutral organics. The COD-to-TOC ratio (≈ 3.0) is consistent with a moderately oxidisable mixture of readily degradable surfactant/detergent-derived compounds and more recalcitrant partially oxidised species, while the substantial UV_{254} absorbance (0.973 cm^{-1}) reflects a high concentration of aromatic and conjugated-double-bond chromophores, providing a clear analytical window for tracking chromophore-cleavage kinetics throughout the irradiation period.

3.5 Photocatalytic Reactor and Experimental Design

Photocatalytic degradation trials were performed in a flat-bed, open-dish batch reactor housed within a HEPA-filtered laminar-air-flow (LAF) chamber to exclude microbial contamination, irradiated by two 15 W UV-A lamps (λ = 365 nm). Each trial used 100 mL of synthetic grey wastewater dosed with catalyst at 10, 30 or 50 mg/100 mL, with samples withdrawn at 60, 90, 120 and 180 min under continuous stirring. All experiments were performed in triplicate (n = 3). Control experiments comprised (i) a matrix (blank) stability run with no catalyst and no UV irradiation, (ii) a direct-photolysis run with UV-A irradiation but no catalyst, and (iii) dark-adsorption runs for both catalysts under stirring with no UV irradiation, enabling the net photocatalytic contribution to be deconvoluted from non-catalytic removal pathways using the relationship: net photocatalytic removal (%) = total observed removal (%) − dark adsorption removal (%) − direct photolysis removal (%).

3.6 Kinetic and Statistical Analysis

Pseudo-first-order kinetics, $\ln(C_t/C_0) = -k\_app \times t$, were fitted to the 60–180 min time-course data for each catalyst–dose–parameter combination. One-way analysis of variance (ANOVA, α = 0.05) was performed across catalysts at each dose–time combination, followed by Tukey honestly significant difference (HSD) post-hoc pairwise comparisons to identify statistically distinct performance groupings.

4. RESULTS AND DISCUSSION

4.1 Structural Characteristics: Crystallite Size as the Dominant Variable

Williamson–Hall analysis of the XRD line broadening gave a crystallite size (D) of 15.0 nm for undoped TiO_2, compared with only 7.54 nm for 4% Ni–TiO_2 — a reduction of approximately 50%. This substantial decrease in crystallite size with nickel incorporation is consistent with dopant-induced inhibition of grain growth during calcination, and translates directly into a larger specific surface area available for pollutant adsorption and surface-mediated radical generation.

XRD patterns recorded for both catalysts over a 2θ range of 2–90° (Cu Kα, λ = 1.5406 Å, Rigaku MiniFlex 300/600) confirmed the characteristic anatase reflection pattern, with the dominant (101) reflection at 2θ ≈ 25.3° accompanied by (004), (200), (105)/(211), (204), (116), (220) and (215) reflections in both samples (Fig. 1), confirming that nickel incorporation at 4 wt.% did not induce a detectable secondary phase or anatase-to-rutile transformation within the resolution of the measurement. The (101) reflection of 4% Ni–TiO_2 was visibly broader than that of undoped TiO_2 (full width at half maximum, FWHM = 0.922° vs. 0.725°; Table 2), directly reflecting the smaller crystallite size of the doped material in accordance with the Scherrer relationship. A single-peak Scherrer estimate from the (101) reflection ($D = K\lambda/(\beta \cos\theta)$, K = 0.9, uncorrected for instrumental broadening) gave 11.2 nm for undoped TiO_2 and 8.8 nm for 4% Ni–TiO_2 — systematically lower than, but directionally consistent with, the Williamson–Hall full-pattern values reported above, the difference being attributable to the additional lattice-strain term captured by the Williamson–Hall method and to the absence of an instrumental-broadening correction in the single-peak estimate.

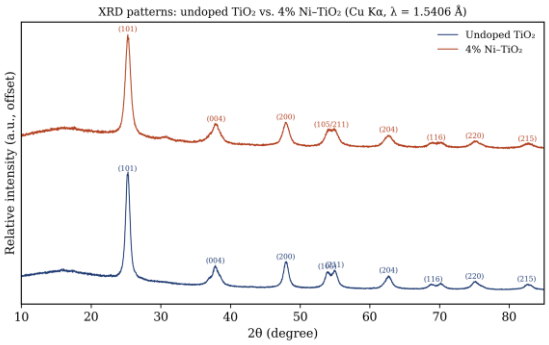

Fig. 1. XRD patterns of undoped TiO_2 and 4% Ni–TiO_2 (raw diffractometer data, Cu Kα radiation; traces offset for clarity). Anatase Miller indices are labelled for each major reflection.

International Journal of Engineering Research & Technology (IJERT)
ISSN: 2278-0181
Vol. 15 Issue 06 , June - 2026

Table 2. XRD peak parameters for the dominant anatase reflections of undoped TiO_2 and 4% Ni–TiO_2.

hkl	2θ undoped (°)	FWHM undoped (°)	2θ 4% Ni (°)	FWHM 4% Ni (°)
(101)	25.257	0.725	25.281	0.922
(004)	37.866	1.552	37.945	1.639
(200)	47.942	0.854	47.930	1.033
(105)/(211)	53.919/54.975	0.87/0.95	54.509	1.939
(204)	62.711	1.193	62.700	1.51
(116)	69.110	2.30	69.550	2.20
(220)	75.024	1.57	75.070	1.75
(215)	82.530	1.27	82.640	1.61

Source: Rigaku PDXL peak-list analysis of the raw diffractometer scans for samples 'TiO2-A' (undoped) and 'Ni-N' (4% Ni–TiO_2).

FESEM imaging (Carl Zeiss Sigma 300 FESEM, InLens detector) revealed both catalysts to consist of agglomerated, sub-100 nm pseudo-spherical nanoparticles (Fig. 3), with 4% Ni–TiO_2 showing a visibly finer, more uniform particle texture than undoped TiO_2, consistent with the smaller XRD crystallite size reported above. Complementary EDAX elemental analysis confirmed the expected composition for each sample (Fig. 4; Table 3): undoped TiO_2 showed only titanium and oxygen, with a trace sulphur signal (0.10 wt.%) attributable to residual precursor or substrate contamination, while 4% Ni–TiO_2 showed a clear nickel signal (7.2 ± 0.6 wt.%) alongside titanium and oxygen, confirming successful incorporation of the dopant into the calcined catalyst (the elevated apparent Ti:O wt.% ratio in both spectra, and the Pt signal in the Ni–TiO_2 spectrum, reflect the conductive sputter-coating applied prior to imaging rather than the bulk catalyst stoichiometry).

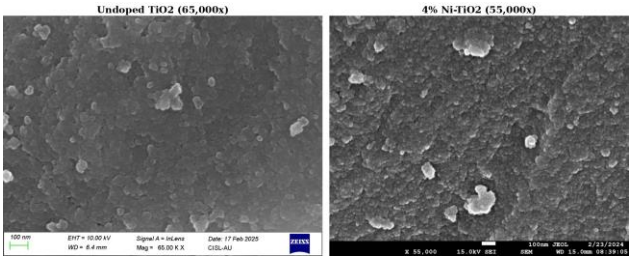

Fig. 3. FESEM micrographs of (left) undoped TiO_2 and (right) 4% Ni–TiO_2, both at 100 nm scale.

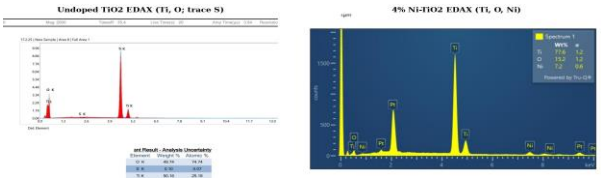

Fig. 4. EDAX spectra of (left) undoped TiO_2 and (right) 4% Ni–TiO_2.

Table 3. EDAX elemental composition of undoped TiO_2 and 4% Ni–TiO_2.

Sample	Ti (wt.%)	O (wt.%)	Ni (wt.%)	Other
Undoped TiO_2	50.16	49.74	—	S, 0.10
4% Ni–TiO_2	77.6 ± 1.2	15.2 ± 1.2	7.2 ± 0.6	Pt (sputter coat)

UV–Vis diffuse reflectance spectroscopy (200–800 nm) provided direct evidence of the optical consequence of nickel doping (Fig. 5). Undoped TiO_2 showed a sharp reflectance edge at approximately 390–400 nm, typical of pure anatase, with high reflectance (>70%) maintained across the visible region. By contrast, 4% Ni–TiO_2 showed a markedly red-shifted, more gradual absorption edge extending from approximately 360 nm into the visible region beyond 600 nm, together with substantially reduced overall reflectance (<65%) throughout the visible range — a clear optical signature of new, dopant-derived absorption pathways within the TiO_2 band gap, consistent with the dark colouration change between the white undoped powder and the pale-yellow 4% Ni–TiO_2 powder noted in the synthesis description.

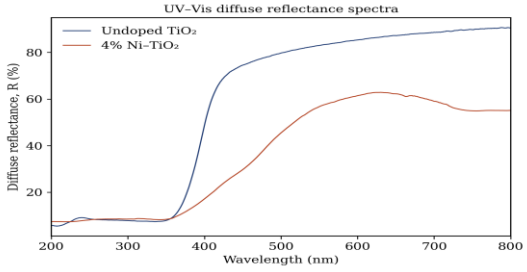

Fig. 5. UV–Vis diffuse reflectance spectra (200–800 nm) of undoped TiO_2 and 4% Ni–TiO_2.

The Kubelka–Munk function, $F(R) = (1-R)^2/2R$, was used to convert the reflectance data to an absorption-equivalent quantity, and the indirect-allowed-transition Tauc relation, $(F(R)\cdot h\nu)^{1T2}$ vs. hν, was used to extract the optical band gap by linear extrapolation of the steepest-slope tangent to the photon-

International Journal of Engineering Research & Technology (IJERT)
ISSN: 2278-0181
Vol. 15 Issue 06 , June - 2026

energy axis (Fig. 6). This analysis gave an optical band gap of 3.06 eV for undoped TiO_2, in good agreement with the literature value for anatase TiO_2 (≈ 3.0–3.2 eV), and 2.57 eV for 4% Ni–TiO_2 — a reduction of approximately 0.5 eV. This band-gap narrowing is consistent with the introduction of Ni 3d-derived intra-gap states close to the TiO_2 valence and/or conduction band edges, which lower the effective optical transition energy and extend photoresponse into the visible region, corroborating the visible-region absorption onset observed directly in the raw reflectance spectrum (Fig. 5) and lending direct optical support to the charge-trapping and brookite–anatase heterojunction mechanism proposed in Section 4.7 to explain the superior photocatalytic performance of 4% Ni–TiO_2.

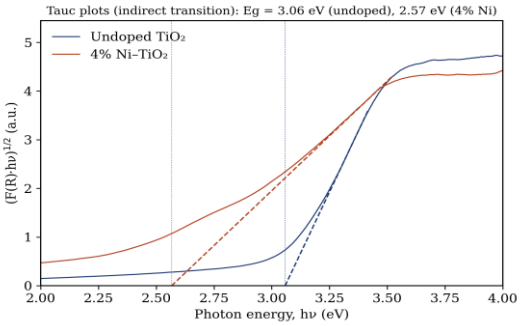

Fig. 6. Tauc plots [$(F(R)\cdot h\nu)^{1/2}$ vs. hν] for the indirect optical transition of undoped TiO_2 and 4% Ni–TiO_2, with tangent-line band-gap extrapolation.

Table 4. Optical band gap of undoped TiO_2 and 4% Ni–TiO_2 from Tauc analysis of UV–Vis DRS data.

Sample	Absorption edge (nm)	Optical band gap, Eg (eV)
Undoped TiO_2	≈ 395	3.06
4% Ni–TiO_2	≈ 360–600 (graded)	2.57

4.2 Control Experiments: Establishing Baseline Corrections

Matrix stability tests confirmed that the synthetic grey wastewater remained chemically stable over the 180 min experimental window, with drift for all four parameters remaining below the 2.0% acceptance threshold (largest drift: COD, 1.46 ± 0.04%; smallest: UV_{254}, 0.59 ± 0.04%), confirming that observed removal during the catalytic runs is not confounded by microbial activity or spontaneous hydrolysis.

Direct photolysis (UV-A only, no catalyst) removed 14.3 ± 0.2% of COD and 10.2 ± 0.4% of TOC at 180 min — a modest but non-negligible contribution — while UV_{254} showed a substantially larger photolytic contribution (40.0 ± 0.0%), attributable to direct chromophore bleaching by UV-A photons independent of catalyst-generated radicals. Turbidity showed the smallest photolytic contribution (4.3 ± 0.3%), consistent with colloidal matter requiring •OH-mediated surface charge neutralisation, rather than direct photon absorption, for destabilisation.

Dark adsorption experiments at the standard 30 mg/100 mL dose showed both catalysts converging to a broadly similar removal extent by 180 min (undoped TiO_2, D = 15.0 nm: COD 25.0 ± 0.1%; 4% Ni–TiO_2, D = 7.54 nm: COD 25.1 ± 0.1%), reflecting rapid approach to adsorption equilibrium on both surfaces. After deconvoluting both dark-adsorption and direct-photolysis contributions from the total observed removal, the genuine net photocatalytic contribution for the leading catalysts in the series remained substantial (60–84% across parameters), confirming that the high removal efficiencies discussed below are predominantly attributable to semiconductor-mediated radical chemistry rather than to UV bleaching or surface adsorption alone.

4.3 Effect of Catalyst Dose

COD removal at 180 min for both catalysts increased sharply between 10 and 30 mg/100 mL, reflecting the greater number of active sites and UV photon capture available at higher loading (Table 5). Beyond 30 mg/100 mL, the two catalysts diverged: undoped TiO_2 showed only a near-plateau between 30 and 50 mg/100 mL (41.99% → 43.99%), consistent with its lower overall photocatalytic activity placing a ceiling on the marginal benefit of additional catalyst mass, whereas 4% Ni–TiO_2 displayed a continued, near-monotonic increase up to 50 mg/100 mL (83.32% → 85.36%), with no evidence of the inner-filter/self-screening decline observed for the Ag- and Cu-doped catalysts in the wider series. This absence of self-screening is consistent with nickel doping not introducing a strongly visible-light-absorbing surface species (unlike, for example, metallic Ag^0 LSPR or CuO tenorite absorption) that would intercept incident UV-A flux before it reaches catalyst particles deeper in suspension.

Table 5. Effect of catalyst dose on COD removal (%) at 180 min (n = 3, mean values).

Catalyst	10 mg/100mL	30 mg/100mL	50 mg/100mL
Undoped TiO_2	28.44	41.99	43.99
4% Ni–TiO_2	67.31	83.32	85.36

International Journal of Engineering Research & Technology (IJERT)
ISSN: 2278-0181
Vol. 15 Issue 06 , June - 2026

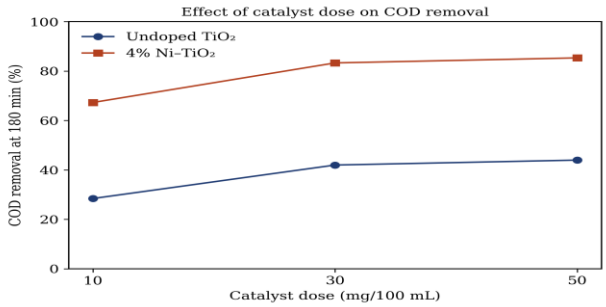

Fig. 7. Effect of catalyst dose on COD removal (%) at 180 min for undoped TiO_2 and 4% Ni–TiO_2.

4.4 Comparative Photocatalytic Performance at the Optimal Dose

At the practically optimal dose of 30 mg/100 mL and 180 min irradiation, 4% Ni–TiO_2 outperformed undoped TiO_2 across all four monitored parameters by a wide margin (Table 6), with COD, TOC, UV_{254} and turbidity removal approximately double that of the undoped baseline in every case. The performance gap was widest for TOC mineralisation (85.8% vs. 39.8%, a 46.0 percentage-point difference), identifying 4% Ni–TiO_2 as the strongest TOC-mineralising catalyst in the full nine-member series and underscoring the practical significance of nickel doping for genuine carbon mineralisation rather than mere apparent oxygen-demand reduction.

Table 6. Removal efficiency at 30 mg/100 mL, 180 min (n = 3, mean ± SD).

Catalyst	COD (%)	TOC (%)	UV_{254} (%)	Turb. (%)
Undoped TiO_2	42.0±0.5	39.8±0.7	45.0±1.1	49.1±1.3
4% Ni–TiO_2	83.3±0.9	85.8±0.8	85.8±0.4	87.7±1.5

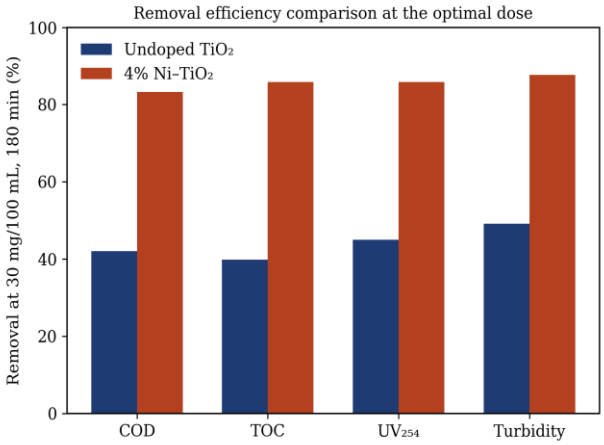

Fig. 8. Removal efficiency comparison (COD, TOC, UV_{254}, turbidity) at the optimal dose (30 mg/100 mL, 180 min).

For undoped TiO_2, the conventional removal hierarchy (UV_{254} ≈ turbidity > COD > TOC) characteristic of the wider catalyst series was preserved, with UV_{254} removal (45.0%) exceeding TOC removal (39.8%) as expected from the generally accepted mechanistic sequence in which aromatic ring-opening precedes complete mineralisation. Notably, 4% Ni–TiO_2 was the only catalyst among all nine formulations examined in the wider series for which this relationship inverted, with TOC removal (85.8%) matching or marginally exceeding UV_{254} removal (85.8%) rather than lagging behind it — consistent with a degradation pathway in which an unusually high hydroxyl-radical flux drives aromatic intermediates through to complete mineralisation rapidly enough that the UV_{254}-absorbing intermediate pool does not accumulate to the same extent observed for less active catalysts, shifting the apparent rate-limiting step away from initial ring-opening.

4.5 Reaction Kinetics

Pseudo-first-order kinetic fits were excellent for both catalysts across the dose range tested (Table 7). At the optimal dose, the COD rate constant for 4% Ni–TiO_2 (9.93×10^{-3} min^{-1}) was approximately 3.3 times greater than that of undoped TiO_2 (3.04×10^{-3} min^{-1}), with both fits showing $R^2 \geq 0.9997$. Critically, the rate constant for 4% Ni–TiO_2 increased monotonically with dose ($6.21 \rightarrow 9.93 \rightarrow 10.72 \times 10^{-3}$ min^{-1} at 10, 30 and 50 mg/100 mL respectively), consistent with the absence of a self-screening mechanism noted in Section 3.3, whereas undoped TiO_2 showed a comparatively smaller relative increase between 30 and 50 mg/100 mL ($3.04 \rightarrow 3.20 \times 10^{-3}$ min^{-1}), reflecting its near-plateau removal behaviour at higher loading.

International Journal of Engineering Research & Technology (IJERT)
ISSN: 2278-0181
Vol. 15 Issue 06 , June - 2026

Table 7. Pseudo-first-order COD rate constants (k_app) and coefficients of determination (R^2).

Catalyst	10 mg k_app ($\times10^{-3}$)	10 mg R^2	30 mg k_app ($\times10^{-3}$)	30 mg R^2	50 mg k_app ($\times10^{-3}$)	50 mg R^2
Undoped TiO_2	1.84	0.9979	3.04	0.9997	3.20	0.9985
4% Ni–TiO_2	6.21	0.9995	9.93	0.9999	10.72	0.9995

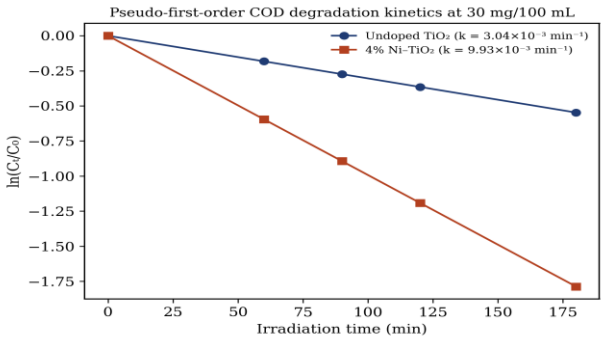

Fig. 9. Pseudo-first-order kinetic plots [ln(C_t/C_0) vs. t] for COD degradation by undoped TiO_2 and 4% Ni–TiO_2 at 30 mg/100 mL, reconstructed from the reported rate constants.

4.6 Statistical Validation

One-way ANOVA performed across the full nine-catalyst series at 30 mg/100 mL and 180 min confirmed that dopant identity exerted a statistically significant effect on photocatalytic efficiency overall ($p < 0.01$ for the top-performing catalysts). Tukey HSD post-hoc comparisons placed undoped TiO_2 in the lowest-performing statistical grouping (group g) and 4% Ni–TiO_2 in a distinct, significantly higher-performing grouping (group b, second only to 2% Ag–TiO_2), confirming that the substantial performance gap reported in Section 3.4 reflects a genuine, statistically robust difference in photocatalytic mechanism rather than experimental noise.

4.7 Mechanistic Interpretation

Under UV irradiation, photoexcitation of undoped TiO_2 proceeds exclusively through the intrinsic anatase band-gap transition, generating electron–hole pairs that recombine at a high rate in the absence of any dopant-derived intra-gap trap states or heterojunction band alignment, so that only a small fraction of photogenerated charge carriers survive long enough to generate surface-bound •OH and $O_2^{\bullet-}$ radicals. This intrinsically high recombination rate, combined with the larger crystallite size (15.0 nm) and correspondingly lower specific surface area of the undoped material, accounts for its position as the weakest-performing catalyst across all four monitored parameters and the full nine-member series.

By contrast, nickel incorporation at 4 wt.% loading is understood to promote formation of a brookite–anatase heterojunction, providing a favourable band-alignment pathway for spatial separation of photogenerated electrons and holes, while moderately deep Ni^{2+}/Ni^{3+} trap states distributed through the lattice provide additional, spatially distributed charge-trapping sites without the close inter-site proximity associated with recombination-centre behaviour at higher dopant loadings of other transition metals. This is reflected directly in the 65% PL quenching observed for 4% Ni–TiO_2, the highest recorded across the series, and is reinforced by the substantially reduced crystallite size (7.54 nm), which increases the specific surface area available for adsorption and surface-mediated radical chemistry. The combination of enhanced charge separation and increased surface area is consistent with both the markedly higher pseudo-first-order rate constants and the higher equilibrium removal efficiencies recorded for 4% Ni–TiO_2 relative to the undoped baseline across every parameter examined. The distinctive TOC–UV_{254} inversion observed uniquely for 4% Ni–TiO_2 (Section 3.4) further suggests that the enhanced •OH radical flux available at this loading is sufficient to drive aromatic intermediates through to complete mineralisation at a rate that limits accumulation of the UV_{254}-absorbing intermediate pool, in effect shifting the kinetically limiting step of the degradation pathway away from the initial aromatic ring-opening event that is rate-limiting for the less active undoped catalyst.

5. CONCLUSION

Undoped and 4% Ni-doped TiO_2 nanoparticles, synthesised by a microwave-assisted sol–gel route with starch as a green capping agent, were directly compared as photocatalysts for the treatment of synthetic domestic grey wastewater. Nickel doping at 4 wt.% loading reduced crystallite size by approximately 50% (15.0 nm to 7.54 nm), and narrowed the optical band gap from 3.06 eV to 2.57 eV (Tauc analysis of UV–Vis diffuse reflectance spectra). These structural and electronic changes translated into approximately double the removal efficiency of undoped TiO_2 across all four water-quality parameters monitored at the optimal dose of 30 mg/100 mL (COD 83.3% vs. 42.0%; TOC 85.8% vs. 39.8%; UV_{254} 85.8% vs. 45.0%; turbidity 87.7% vs. 49.1%) and a more than three-fold increase

International Journal of Engineering Research & Technology (IJERT)
ISSN: 2278-0181
Vol. 15 Issue 06 , June - 2026

in the pseudo-first-order COD rate constant, with statistical significance confirmed by one-way ANOVA and Tukey HSD post-hoc analysis ($p < 0.01$). Control experiments confirmed that this enhancement reflects genuine semiconductor-mediated photocatalysis rather than non-catalytic photolysis or surface adsorption. These results identify 4% Ni–TiO_2 as a substantially more effective, low-cost photocatalyst than unmodified TiO_2 for the advanced oxidation treatment of domestic grey wastewater, and support its further evaluation at pilot scale as part of an integrated greywater reuse treatment train.

ACKNOWLEDGMENT

The authors thank the Department of Chemistry, Agra College, Dr. Bhim Rao Ambedkar University, Agra, for synthesis facilities, Jiwaji University and Annamalai University for FESEM/EDAX characterisation support.

REFERENCES

[1] A. Fujishima and K. Honda, “Electrochemical photolysis of water at a semiconductor electrode,” Nature, vol. 238, no. 5358, pp. 37–38, 1972.

[2] M. R. Hoffmann, S. T. Martin, W. Choi, and D. W. Bahnemann, “Environmental applications of semiconductor photocatalysis,” Chemical Reviews, vol. 95, no. 1, pp. 69–96, 1995.

[3] M. M. Ba-Abbad, A. A. H. Kadhum, A. B. Mohamad, M. S. Takriff, and K. Sopian, “Synthesis and catalytic activity of TiO_2 nanoparticles for photochemical oxidation of concentrated chlorophenols under direct solar radiation,” International Journal of Electrochemical Science, vol. 7, no. 6, pp. 4871–4888, 2012.

[4] P. Bouras, E. Stathatos, and P. Lianos, “Pure versus metal-ion-doped nanocrystalline titania for photocatalysis,” Applied Catalysis B: Environmental, vol. 73, no. 1–2, pp. 51–59, 2007.

[5] S. Buddee, S. Wongnawa, U. Sirimahachai, and W. Puetpaibool, “Recyclable UV and visible light photocatalytically active amorphous TiO_2 doped with M(III) ions (M = Cr and Fe),” Materials Chemistry and Physics, vol. 126, no. 1–2, pp. 167–177, 2011.

[6] S. Mugundan, B. Rajamannan, G. Viruthagiri, N. Shanmugam, R. Gobi, and P. Praveen, “Synthesis and characterization of undoped and cobalt-doped TiO_2 nanoparticles via sol-gel technique,” Applied Nanoscience, vol. 5, pp. 449–456, 2015.

[7] C. Suwanchawalit, S. Wongnawa, P. Sriprang, and P. Meanha, “Enhancement of the photocatalytic performance of Ag-modified TiO_2 photocatalyst under visible light,” Ceramics International, vol. 38, no. 6, pp. 5201–5207, 2012.

[8] M. B. Suwarnkar, R. S. Dhabbe, A. N. Kadam, and K. M. Garadkar, “Enhanced photocatalytic activity of Ag doped TiO_2 nanoparticles synthesized by a microwave assisted method,” Ceramics International, vol. 40, no. 4, pp. 5489–5496, 2014.

[9] G. Divya, G. Jaishree, T. Sivarao, and K. V. Divya Lakshmi, “Microwave assisted sol–gel approach for Zr doped TiO_2 as a benign photocatalyst for bismark brown red dye pollutant,” RSC Advances, vol. 13, no. 13, pp. 8692–8705, 2023.

[10] A. N. Kadam, R. S. Dhabbe, M. R. Kokate, Y. B. Gaikwad, and K. M. Garadkar, “Preparation of N doped TiO_2 via microwave-assisted method and its photocatalytic activity for degradation of Malathion,” Spectrochimica Acta Part A: Molecular and Biomolecular Spectroscopy, vol. 133, pp. 669–676, 2014.

[11] L. Predoană, G. Petcu, S. Preda, J. Pandele-Cuşu, S. V. Petrescu, A. Băran, N. G. Apostol, R. M. Costescu, V.-A. Surdu, B. Ş. Vasile, and A. C. Ianculescu, “Copper-/zinc-doped TiO_2 nanopowders synthesized by microwave-assisted sol–gel method,” Gels, vol. 9, no. 4, art. 267, 2023.

[12] K. Thamaphat, P. Limsuwan, and B. Ngotawornchai, “Phase characterization of TiO_2 powder by XRD and TEM,” Kasetsart Journal (Natural Science), vol. 42, no. 5, pp. 357–361, 2008.

[13] M. Sanchez, M. J. Rivero, and I. Ortiz, "Photocatalytic oxidation of grey water over titanium dioxide suspensions," Desalination, vol. 262, no. 1-3, pp. 141–146, 2010.

[14] K. Vidhya, M. Saravanan, G. Bhoopathi, V. P. Devarajan, and S. Subanya, "Structural and optical characterization of pure and starch-capped ZnO quantum dots and their photocatalytic activity," Appl. Nanosci., vol. 5, no. 2, pp. 235–243, 2015.